AIAA-2003-0324

Calculation of the Ideal MHD Equations by the CESE Method without Special Treatment for the Divergence-Free Constraint of Magnetic Field

Moujin Zhang[1], S.-T. John Yu[2]
Mechanical Engineering Department
Wayne State University, Detroit, MI 48202

Sin-Chung Chang[3] and Isaiah Blankson[4]
NASA Glenn Research Center
Cleveland, OH 44135

Abstract

In this paper, we introduce a new numerical approach to solve two spatial dimensional ideal magneto-hydrodynamic (MHD) equations. By treating space and time as one entity, the ideal MHD equations are formulated in a space-time integral form, and are solved by the Space-Time Conservation Element and Solution Element (CESE) method. Contrast to the modern upwind methods, no reconstruction procedure or Riemann solver is needed in the present approach. The computational logic and operational count of the present approach are much simpler and more efficient. Moreover, no special treatment has been employed to maintain the divergence-free condition for the magnetic field. Nevertheless, the $\nabla \cdot \mathbf{B} = 0$ constraint has been faithfully maintained in smooth region. In regions near shocks, the magnitude of $|\nabla \cdot \mathbf{B}|$ is bounded. Two benchmark problems have been calculated. Present results of propagating MHD shock and expansion waves in two spatial dimensions for long-term evolution showed remarkable numerical resolution.

[1] Research Associate, Email: mzhang@me1.eng.wayne.edu
[2] Associate Professor, Email: styu@me1.eng.wayne.edu
[3] Senior Aerospace Scientist,
Email: sin-chung.chang@lerc.nasa.gov
[4] Senior Technologist, Email: Isaiah.blankson@lerc.nasa.gov

1. Introduction

Recently, the computational magneto-hydrodynamics (MHD) has drawn significant attention due to a growing interest in plasma-based aerodynamics, including flow manipulation through plasma, on-board power generation, and drag reduction in hypersonic vehicles. The flow phenomena in plasma is much more complex than that in gas dynamics. While many numerical modules developed for gas dynamics could be used in solving the MHD equations, numerical solution of the MHD equations involves unique requirements and thus poses a greater challenge than the CFD for gas dynamics.

To date, efforts in developing viable MHD solvers have been focused on the use of modern upwind method [1-10]. Thus the Riemann solvers based on the knowledge on the eigensystem of the governing equations has been a critical issue. For computational efficiency, approximated Riemann solvers have been employed. Although this approach has been successful for ideal MHD equations, extension to more complex MHD processes will be difficult due to the fact that Riemann solutions to complex MHD waves have been scant.

Another important issue is to maintain the divergence free condition for the magnetic field, i.e., $\nabla \cdot \mathbf{B} = 0$, at all time for all locations. Analytically, this constraint is ensured if it is satisfied at the initial condition. However, it has been a difficult task to maintain this constraint numerically. Violating the $\nabla \cdot \mathbf{B} = 0$ constraint and allowing the error to be accumulated over a period of time may result in erroneous solutions, which in turn may lead to numerical instability. Special treatments are required to numerically enforce the constraint for problems in multiple space dimensions.

In the past, numerical procedures for maintaining the constraint can be categorized into three groups: (i) the projection procedure [3], (ii) the eight-wave formulation [4], and (iii) the constrained transport procedures [5-9]. These three approaches were assessed and compared by Toth [9]. In general, special treatments have been indispensable for MHD computation based on the use of the upwind schemes.

Due to the complexity of the MHD problems, highly accurate but simple method is desired. This is particularly important for extending the solvers to model complex MHD processes, in which the model equations could include multiple fluids with chemical reactions. In the present paper, we report the numerical solution of the ideal MHD equations by the Space-Time Conservation Element and Solution Element (CESE) method as the first step for the development of a general numerical framework for complex MHD models. We shall show that we do not need to construct a Riemann solver for the complex MHD equations, and we do not need to employ a special treatment to numerically enforce $\nabla \cdot \mathbf{B} = 0$ constraint.

In a series of publications [11-17], Chang and coworkers have successfully developed the CESE method for linear and nonlinear convection-diffusion equations in one, two, and three spatial dimensions. Numerous results, obtained by using the CESE method, have been reported in the cited references, including flows with steady and moving shock, rarefaction waves, and acoustic waves, flows dominated by vortices, detonation waves, shock/acoustic waves/vortices interactions, dam-break flows, hydraulic jump, cavitations, and the turbulent flows with embedded sprays.

The rest of the paper is organized as follows. Section 2 illustrates the model equations for two-dimensional MHD problem. Section 3 presents the CESE method for two-dimensional MHD equations. In Section 4, numerical results and analysis are presented. We then offer concluding remarks and provide cited references.

2. Model Equations

The two-dimensional ideal MHD equations in the conservation form are

$$\frac{\partial \mathbf{u}}{\partial t} + \frac{\partial \mathbf{f}}{\partial x} + \frac{\partial \mathbf{g}}{\partial y} = 0 , \tag{2.1}$$

where

$$\begin{aligned} \mathbf{u} &= \left(\rho, \rho u, \rho v, \rho w, e, B_x, B_y, B_z\right)^T \\ &= \left(u_1, u_2, u_3, u_4, u_5, u_6, u_7, u_8\right)^T , \end{aligned} \tag{2.2}$$

$$\begin{aligned} \mathbf{f}(\mathbf{u}) &= \begin{pmatrix} \rho u \\ \rho u^2 + p_0 - B_x{}^2 \\ \rho uv - B_x B_y \\ \rho uw - B_x B_z \\ (e + p_0)u - B_x\left(uB_x + vB_y + wB_z\right) \\ 0 \\ uB_y - vB_x \\ uB_z - wB_x \end{pmatrix} \\ &= \left(f_1, f_2, f_3, f_4, f_5, f_6, f_7, f_8\right)^T \end{aligned} \tag{2.3}$$

and

$$\begin{aligned} \mathbf{g}(\mathbf{u}) &= \begin{pmatrix} \rho v \\ \rho vu - B_y B_x \\ \rho v^2 + p_0 - B_y^2 \\ \rho vw - B_y B_z \\ (e + p_0)v - B_y\left(uB_x + vB_y + wB_z\right) \\ vB_x - uB_y \\ 0 \\ vB_z - wB_y \end{pmatrix} \\ &= \left(g_1, g_2, g_3, g_4, g_5, g_6, g_7, g_8\right)^T \end{aligned} \tag{2.4}$$

The specific total energy e is

$$\begin{aligned} e = {} & p/(\gamma - 1) + \rho\left(u^2 + v^2 + w^2\right)/2 \\ & + \left(B_x^2 + B_y^2 + B_z^2\right)/2 \end{aligned} .$$

The total pressure is

$$p_0 = p + \left(B_x^2 + B_y^2 + B_z^2\right)/2 .$$

In addition to the above equations, the magnetic field satisfies the divergence free constraint $\nabla \cdot \mathbf{B} = 0$.

3. The CESE Method

The MHD equations in two spatial dimensions can be expressed as

$$\frac{\partial u_m}{\partial t} + \frac{\partial f_m}{\partial x} + \frac{\partial g_m}{\partial y} = 0 , \tag{3.1}$$

for m = 1, 2,…., 8, where u_m, f_m and g_m are flow variables, Eq. (2.2), and fluxes in x- and y- directions, Eqs. (2.3-4), respectively. Let $x_1 = x, x_2 = y$ and $x_3 = t$ be the coordinates of a three-dimensional Eucilidean space E_3. Equation (3.1) becomes the divergence free condition in E_3,

$$\nabla \cdot \mathbf{h}_m = 0, \tag{3.2}$$

where $\mathbf{h}_m = (f_m, g_m, u_m)$ are the current density vectors in E_3. By using Gauss' divergence theorem in E_3, we have

$$\int_V \nabla \cdot \mathbf{h}_m dV = \oint_{S(V)} \mathbf{h}_m \cdot d\mathbf{s} = 0, \tag{3.3}$$

for m = 1, 2,…., 8, where $S(V)$ is the boundary of an arbitrary space-time region V in E_3 and $d\mathbf{s} = \mathbf{n} d\sigma$, where $d\sigma$ and $\mathbf{n}$ are the area and the outward unit normal vector of a surface element on $S(V)$.

The SE and CE in a two spatial dimensions are shown in Fig. 1. For the sake of conciseness, we present the two-dimensional CESE method based on the use of a uniform mesh. In Fig. 1a, the spatial domain is covered by congruent triangles. The centorid of each triangle is marked by either a hollow circle or a solid circle. If the centroid of a triangle is marked by a solid (hollow) circle, the centorids of the three neighboring triangles are marked by hollow (solid) circles. In Fig. 1a, point G, centorid of ΔBDF, is marked by a solid circle, while the points A, C and E are the centorids of ΔFMB, ΔBJD, and ΔDLF and are marked by hollow circles. Let j, k and n be indexes for x, y and t, respectively. Points A, B, C, D, E, F and G are at the time level $n-1/2$. A', B', C', D', E', F' and G' are at the time level n. A'', B'', C'', D'', E'', F'' and G'' are at the time level $n+1/2$. The centorids are in a staggered arrangement in E_3. Points G', G, A, C and E are marked by (j, k, n), $(j, k, n-1/2)$, $(j1, k1, n-1/2)$, $(j2, k2, n-1/2)$ and $(j3, k3, n-1/2)$ respectively. As presented in Fig. 1c, the solution element $SE(j, k, n)$ for point (j, k, n) is the union of four planes, hexagon $A'B'C'D'E'F'$, quadrilateral $B''BGG''$, quadrilateral $D''DGG''$ and quadrilateral $F''FGG''$, and their intermediate neighborhood.

There are three SEs, i.e., $SE(j1, k1, n-1/2)$, $SE(j2, k2, n-1/2)$ and $SE(j3, k3, n-1/2)$ associated with points A, C and E respectively. The surfaces of the four SEs form three CEs for point (j, k, n). They are quadrilateral cylinders $ABGFA'B'G'F'$, $CDGBC'D'G'B'$ and $EFGDE'F'G'D'$, and are referred to as $CE_1(j,k,n)$, $CE_2(j,k,n)$ and $CE_3(j,k,n)$, respectively. $CE(j,k,n)$ is the union of $CE_1(j,k,n)$, $CE_2(j,k,n)$ and $CE_3(j,k,n)$.

Inside $SE(j,k,n)$, the first-order Taylor series expansion is employed to descritize the flow variables and fluxes:

$$u_m^*(x,y,t;j,k,n) = (u_m)_{j,k}^n + (u_{mx})_{j,k}^n (x - x_{j,k}) + (u_{my})_{j,k}^n (y - y_{j,k}) + (u_{mt})_{j,k}^n (t - t^n)' \tag{3.4}$$

$$f_m^*(x,y,t;j,k,n) = (f_m)_{j,k}^n + (f_{mx})_{j,k}^n (x - x_{j,k}) + (f_{my})_{j,k}^n (y - y_{j,k}) + (f_{mt})_{j,k}^n (t - t^n)' \tag{3.5}$$

$$g_m^*(x,y,t;j,k,n) = (g_m)_{j,k}^n + (g_{mx})_{j,k}^n (x - x_{j,k}) + (g_{my})_{j,k}^n (y - y_{j,k}) + (g_{mt})_{j,k}^n (t - t^n), \tag{3.6}$$

for m = 1, 2,…., 8. Eq. (3.3) is then approximated by

$$\oint_{S(V)} \mathbf{h}_m^* \cdot d\mathbf{s} = 0, \tag{3.7}$$

where $\mathbf{h}_m^* = (f_m^*, g_m^*, u_m^*)$. At point (j,k,n), we let

$$(u_{mt})_{j,k}^n = -(f_{mx})_{j,k}^n - (g_{my})_{j,k}^n, \tag{3.8}$$

for m = 1, 2,…., 8. To proceed, let $f_{m,l}$ and $g_{m,l}$ be the entries of Jacobian matrixes **F** and **G** which are presented in Appendix**,** i.e.,

$$f_{m,l} = \frac{\partial f_m}{\partial u_l} \quad \text{and} \quad g_{m,l} = \frac{\partial g_m}{\partial u_l}, \tag{3.9}$$

for m, l = 1, 2,…., 8. Aided by the chain rule, we have,

$$\left(f_{mx}\right)_j^n = \sum_{l=1}^{8} \left(f_{m,l}\right)_{j,k}^n \left(u_{lx}\right)_{j,k}^n , \tag{3.10}$$

$$\left(f_{my}\right)_j^n = \sum_{l=1}^{8} \left(f_{m,l}\right)_{j,k}^n \left(u_{ly}\right)_{j,k}^n , \tag{3.11}$$

$$\left(g_{mx}\right)_{j,k}^n = \sum_{l=1}^{8} \left(g_{m,l}\right)_{j,k}^n \left(u_{lx}\right)_{j,k}^n , \tag{3.12}$$

and

$$\left(g_{my}\right)_{j,k}^n = \sum_{l=1}^{8} \left(g_{m,l}\right)_{j,k}^n \left(u_{ly}\right)_{j,k}^n . \tag{3.13}$$

Aided by Eqs. (3.10-13), Eq. (3.8) can be recast to

$$\left(u_{mt}\right)_j^n = -\sum_{l=1}^{8} \left(f_{m,l}\right)_{j,k}^n \left(u_{lx}\right)_{j,k}^n - \sum_{l=1}^{8} \left(g_{m,l}\right)_{j,k}^n \left(u_{ly}\right)_{j,k}^n , \tag{3.14}$$

Aided by the chain rule and Eqs. (3.14), $\left(f_{mt}\right)_{j,k}^n$ and $\left(g_{mt}\right)_{j,k}^n$ can be expressed as,

$$\begin{aligned} \left(f_{mt}\right)_j^n &= \sum_{l=1}^{8} \left(f_{m,l}\right)_{j,k}^n \left(u_{lt}\right)_{j,k}^n \\ &= -\sum_{l=1}^{8} \left(f_{m,l}\right)_j^n \sum_{r=1}^{8} \left(f_{l,r}\right)_{j,k}^n \left(u_{rx}\right)_{j,k}^n \\ &\quad - \sum_{l=1}^{8} \left(f_{m,l}\right)_j^n \sum_{r=1}^{8} \left(g_{l,r}\right)_{j,k}^n \left(u_{ry}\right)_{j,k}^n , \end{aligned} \tag{3.15}$$

$$\begin{aligned} \left(g_{mt}\right)_{j,k}^n &= \sum_{l=1}^{8} \left(g_{m,l}\right)_{j,k}^n \left(u_{lt}\right)_{j,k}^n \\ &= -\sum_{l=1}^{8} \left(g_{m,l}\right)_{j,k}^n \sum_{r=1}^{8} \left(f_{l,r}\right)_{j,k}^n \left(u_{rx}\right)_{j,k}^n \\ &\quad - \sum_{l=1}^{8} \left(g_{m,l}\right)_{j,k}^n \sum_{r=1}^{8} \left(g_{l,r}\right)_{j,k}^n \left(u_{ry}\right)_{j,k}^n , \end{aligned} \tag{3.16}$$

for m = 1, 2,…., 8.

Aided by Eqs. (3.9-13), Eqs. (3.4-6) could fully specify the distribution of u_m^*, f_m^* and g_m^* inside $SE(j,k,n)$ when values of $\left(u_m\right)_{j,k}^n$ $\left(u_{mx}\right)_{j,k}^n$ and $\left(u_{my}\right)_{j,k}^n$ are known. For each m, there are three unknowns, $\left(u_m\right)_{j,k}^n$, $\left(u_{mx}\right)_{j,k}^n$ and $\left(u_{my}\right)_{j,k}^n$. Three CEs, i.e., $CE_1(j,k,n)$, $CE_2(j,k,n)$ and $CE_3(j,k,n)$, associated with point (j,k,n) are constructed to provide three algebraic equations to solve the unknowns.

To proceed, we calculate the flux leaving surfaces of CEs. Consider $CE_1(j,k,n)$, quadrilateral cylinder $ABGFA'B'G'F'$. The surfaces of $CE_1(j,k,n)$ consist of two groups. As shown in Fig. 1d, quadrilaterals $FGG'F'$, $A'B'G'F'$ and $BGG'B'$ belong to $SE(j,k,n)$, and quadrilaterals $ABGF$, $ABB'A'$ and $AFF'A'$ belong to $SE(j1,k1,n-1/2)$. Let S be the area of the quadrilaterals. Let $(x_{cen}, y_{cen}, t_{cen})$ be the coordinates of the centroid of each area. Over each area, let the outward normal vector be **n**, and the surface vector **s** = **n** S.

The flux leaving a surface is equal to the scalar product between the vector $\mathbf{h}_m^* = \left(f_m^*, g_m^*, u_m^*\right)$, evaluated at surface's centroid, and the surface vector **s**. For quadrilateral $A'B'G'F'$ in E_3, its surface vector is

$$\mathbf{s}_{A'B'G'F'} = (0,\, 0,\, S_{q1}), \tag{3.17}$$

and the coordinates of its centroid O, as shown in Fig. 1d, are

$$(x_O, y_O, t_O) = \left(x_{q1}, y_{q1}, t^n\right), \tag{3.18}$$

where S_{q1} and (x_{q1}, y_{q1}) are area and centroid's spatial coordinates of quadrilateral $A'B'G'F'$. The flux leaving the surface $A'B'G'F'$ is

$$\begin{aligned} &\left(FLUX_m\right)_{A'B'G'F'} \\ &= S_{q1}\left[\left(u_m\right)_{j,k}^n + \left(x_{q1} - x_G\right)\left(u_{mx}\right)_{j,k}^n \right. \\ &\qquad \left. + \left(y_{q1} - y_G\right)\left(u_{my}\right)_{j,k}^n\right] \end{aligned} \tag{3.19}$$

For quadrilateral $FGG'F'$, its surface vector is

$$\mathbf{s}_{FGG'F'} = \frac{\Delta t}{2}\left(y_F - y_G, x_G - x_F, 0\right), \tag{3.20}$$

and the coordinates of its centroid Q, as shown in Fig. 1d, are

$$\left(x_Q, y_Q, t_Q\right)=\left(\frac{x_F+x_G}{2}, \frac{y_F+y_G}{2}, t^n-\frac{\Delta t}{4}\right) \tag{3.21}$$

The flux leaving the surface $FGG'F'$ is

$$\begin{aligned}
&\left(FLUX_m\right)_{FGG'F'} = \\
&\frac{\Delta t}{2}\left(y_F-y_G\right)\left[\left(f_m\right)_{j,k}^n+\frac{\left(x_F-x_G\right)}{2}\left(f_{mx}\right)_{j,k}^n\right. \\
&\left.+\frac{\left(y_F-y_G\right)}{2}\left(f_{my}\right)_{j,k}^n-\frac{\Delta t}{4}\left(f_{mt}\right)_{j,k}^n\right] \\
&+\frac{\Delta t}{2}\left(x_G-x_F\right)\left[\left(g_m\right)_{j,k}^n+\frac{\left(x_F-x_G\right)}{2}\left(g_{mx}\right)_{j,k}^n\right. \\
&\left.+\frac{\left(y_F-y_G\right)}{2}\left(g_{my}\right)_{j,k}^n-\frac{\Delta t}{4}\left(g_{mt}\right)_{j,k}^n\right].
\end{aligned} \tag{3.22}$$

For quadrilateral $BGG'B'$, its surface vector is

$$\mathbf{s}_{BGG'B'}=\frac{\Delta t}{2}\left(\, y_G-y_B, x_B-x_G, 0\,\right), \tag{3.23}$$

and the coordinates of its centroid P, as shown in Fig. 1d, are

$$\left(x_P, y_P, t_P\right)=\left(\frac{x_B+x_G}{2}, \frac{y_B+y_G}{2}, t^n-\frac{\Delta t}{4}\right) \tag{3.24}$$

The flux leaving the surface $BGG'B'$ is

$$\begin{aligned}
&\frac{\Delta t}{2}\left(y_G-y_B\right)\left[\left(f_m\right)_{j,k}^n+\frac{\left(x_B-x_G\right)}{2}\left(f_{mx}\right)_{j,k}^n\right. \\
&\left.+\frac{\left(y_B-y_G\right)}{2}\left(f_{my}\right)_{j,k}^n-\frac{\Delta t}{4}\left(f_{mt}\right)_{j,k}^n\right] \\
&+\frac{\Delta t}{2}\left(x_B-x_G\right)\left[\left(g_m\right)_{j,k}^n+\frac{\left(x_B-x_G\right)}{2}\left(g_{mx}\right)_{j,k}^n\right. \\
&\left.+\frac{\left(y_B-y_G\right)}{2}\left(g_{my}\right)_{j,k}^n-\frac{\Delta t}{4}\left(g_{mt}\right)_{j,k}^n\right]
\end{aligned} \tag{3.25}$$

The flux leaving three surfaces belonging to $SE(j,k,n)$ is the sum of Eqs. (3.19), (3.22) and (3.25). Similar calculation could be performed to obtain fluxes leaving three surfaces of $SE\left(j1,k1,n-1/2\right)$, and we have

$$\begin{aligned}
&\left(flux_m\right)_1^{n-1/2} \\
&=-S_{q1}\left[\left(u_m\right)_{j1,k1}^{n-1/2}+\left(x_{q1}-x_A\right)\left(u_{mx}\right)_{j1,k1}^{n-1/2}\right. \\
&\qquad\left.+\left(y_{q1}-y_A\right)\left(u_{my}\right)_{j1,k1}^{n-1/2}\right] \\
&\quad+\frac{\Delta t}{2}\left(y_B-y_F\right)\left(f_m\right)_{j1,k1}^{n-1/2} \\
&\quad+\frac{\Delta t}{4}\left[\left(x_B-x_A\right)\left(y_B-y_A\right)\right. \\
&\qquad\left.-\left(x_F-x_A\right)\left(y_F-y_A\right)\right]\left(f_{mx}\right)_{j1,k1}^{n-1/2} \\
&\quad+\frac{\Delta t}{4}\left[\left(y_B-y_A\right)^2-\left(y_F-y_A\right)^2\right]\left(f_{my}\right)_{j1,k1}^{n-1/2} \\
&\quad+\frac{(\Delta t)^2}{8}\left(y_B-y_F\right)\left(f_{mt}\right)_{j1,k1}^{n-1/2} \\
&+\frac{\Delta t}{2}\left(x_F-x_B\right)\left(g_m\right)_{j1,k1}^{n-1/2} \\
&+\frac{\Delta t}{4}\left[\left(x_F-x_A\right)^2-\left(x_B-x_A\right)^2\right]\left(g_{mx}\right)_{j1,k1}^{n-1/2} \\
&+\frac{\Delta t}{4}\left[\left(x_F-x_A\right)\left(y_F-y_A\right)\right. \\
&\qquad\left.-\left(x_B-x_A\right)\left(y_B-y_A\right)\right]\left(g_{my}\right)_{j1,k1}^{n-1/2} \\
&+\frac{(\Delta t)^2}{8}\left(x_F-x_B\right)\left(g_{mt}\right)_{j1,k1}^{n-1/2}.
\end{aligned} \tag{3.26}$$

With the aid of Eqs. (3.19), (3.22), (3.25) and (3.26), the flux conservation over $CE_1(j,k,n)$ is

$$\begin{aligned}
&S_{q1}\left[\left(u_m\right)_{j,k}^n+\left(x_{q1}-x_G\right)\left(u_{mx}\right)_{j,k}^n\right. \\
&\qquad\left.+\left(y_{q1}-y_G\right)\left(u_{my}\right)_{j,k}^n\right] \\
&\quad+\frac{\Delta t}{2}\left(y_F-y_B\right)\left(f_m\right)_{j,k}^n \\
&\quad+\frac{\Delta t}{4}\left[\left(x_F-x_G\right)\left(y_F-y_G\right)\right. \\
&\quad\left.-\left(x_B-x_G\right)\left(y_B-y_G\right)\right]\left(f_{mx}\right)_{j,k}^n \\
&\quad+\frac{\Delta t}{4}\left[\left(y_F-y_G\right)^2-\left(y_B-y_G\right)^2\right]\left(f_{my}\right)_{j,k}^n \\
&\quad-\frac{(\Delta t)^2}{8}\left(y_F-y_B\right)\left(f_{mt}\right)_{j,k}^n \\
&\quad+\frac{\Delta t}{2}\left(x_B-x_F\right)\left(g_m\right)_{j,k}^n \\
&\quad+\frac{\Delta t}{4}\left[\left(x_B-x_G\right)^2-\left(x_F-x_G\right)^2\right]\left(g_{mx}\right)_{j,k}^n
\end{aligned}$$

$$+\frac{\Delta t}{4}\left[\left(x_B-x_G\right)\left(y_B-y_G\right)\right.$$
$$\left.-\left(x_F-x_G\right)\left(y_F-y_G\right)\right]\left(g_{my}\right)_{j,k}^{n}$$
$$-\frac{(\Delta t)^2}{8}\left(x_B-x_F\right)\left(g_{mt}\right)_{j,k}^{n}+\left(flux_m\right)_1^{n-1/2}=0\,, \tag{3.27}$$

for m = 1, 2,…., 8, where $\left(flux_m\right)_1^{n-1/2}$ is provided in Eq. (3.26).

Similarly, the flux conservation over $CE_2(j,k,n)$ is

$$S_{q2}\left[\left(u_m\right)_{j,k}^{n}+\left(x_{q2}-x_G\right)\left(u_{mx}\right)_{j,k}^{n}\right.$$
$$\left.+\left(y_{q2}-y_G\right)\left(u_{my}\right)_{j,k}^{n}\right]$$
$$+\frac{\Delta t}{2}\left(y_B-y_D\right)\left(f_m\right)_{j,k}^{n}$$
$$+\frac{\Delta t}{4}\left[\left(x_B-x_G\right)\left(y_B-y_G\right)\right.$$
$$\left.-\left(x_D-x_G\right)\left(y_D-y_G\right)\right]\left(f_m\right)_{j,k}^{n}$$
$$+\frac{\Delta t}{4}\left[\left(y_B-y_G\right)^2-\left(y_D-y_G\right)^2\right]\left(f_{my}\right)_{j,k}^{n}$$
$$-\frac{(\Delta t)^2}{8}\left(y_B-y_D\right)\left(f_{mt}\right)_{j,k}^{n}$$
$$+\frac{\Delta t}{2}\left(x_D-x_B\right)\left(g_m\right)_{j,k}^{n}$$
$$+\frac{\Delta t}{4}\left[\left(x_D-x_G\right)^2-\left(x_B-x_G\right)^2\right]\left(g_{mx}\right)_{j,k}^{n}$$
$$+\frac{\Delta t}{4}\left[\left(x_D-x_G\right)\left(y_D-y_G\right)\right.$$
$$\left.-\left(x_B-x_G\right)\left(y_B-y_G\right)\right]\left(g_{my}\right)_{j,k}^{n}$$
$$-\frac{(\Delta t)^2}{8}\left(x_D-x_B\right)\left(g_{mt}\right)_{j,k}^{n}+\left(flux_m\right)_2^{n-1/2}=0 \tag{3.28}$$

where S_{q2} is the area of the quadrilateral $B'C'D'G'$, and $\left(x_{q2},y_{q2}\right)$ are the spatial coordinates of its centroid. In Eq. (3.28), the fluxes leaving three surfaces of $SE(j2,k2,n-1/2)$ are

$$\left(flux_m\right)_2^{n-1/2}=$$
$$-S_{q2}\left[\left(u_m\right)_{j2,k2}^{n-1/2}+\left(x_{q2}-x_C\right)\left(u_{mx}\right)_{j2,k2}^{n-1/2}\right.$$
$$\left.+\left(y_{q1}-y_C\right)\left(u_{my}\right)_{j2,k2}^{n-1/2}\right]$$
$$+\frac{\Delta t}{4}\left(y_D-y_B\right)\left(f_m\right)_{j2,k2}^{n-1/2}$$
$$+\frac{\Delta t}{4}\left[\left(x_D-x_C\right)\left(y_D-y_C\right)\right.$$
$$\left.-\left(x_B-x_C\right)\left(y_B-y_C\right)\right]\left(f_{mx}\right)_{j2,k2}^{n-1/2}$$
$$+\frac{\Delta t}{4}\left[\left(y_D-y_C\right)^2-\left(y_B-y_C\right)^2\right]\left(f_{my}\right)_{j2,k2}^{n-1/2}$$
$$+\frac{(\Delta t)^2}{8}\left(y_D-y_B\right)\left(f_{mt}\right)_{j2,k2}^{n-1/2}$$
$$+\frac{\Delta t}{2}\left(x_B-x_D\right)\left(g_m\right)_{j2,k2}^{n-1/2}$$
$$+\frac{\Delta t}{4}\left[\left(x_B-x_C\right)^2-\left(x_D-x_C\right)^2\right]\left(g_{mx}\right)_{j2,k2}^{n-1/2}$$
$$+\frac{\Delta t}{4}\left[\left(x_B-x_C\right)\left(y_B-y_C\right)\right.$$
$$\left.-\left(x_D-x_C\right)\left(y_D-y_C\right)\right]\left(g_{my}\right)_{j1,k1}^{n-1/2}$$
$$+\frac{(\Delta t)^2}{8}\left(x_B-x_D\right)\left(g_{mt}\right)_{j1,k1}^{n-1/2}. \tag{3.29}$$

Similarly, the flux conservation over $CE_3(j,k,n)$ is

$$S_{q3}\left[\left(u_m\right)_{j,k}^{n}+\left(x_{q3}-x_G\right)\left(u_{mx}\right)_{j,k}^{n}\right.$$
$$\left.+\left(y_{q3}-y_G\right)\left(u_{my}\right)_{j,k}^{n}\right]$$
$$+\frac{\Delta t}{2}\left(y_D-y_F\right)\left(f_m\right)_{j,k}^{n}$$
$$+\frac{\Delta t}{4}\left[\left(x_D-x_G\right)\left(y_D-y_G\right)\right.$$
$$\left.-\left(x_F-x_G\right)\left(y_F-y_G\right)\right]\left(f_{mx}\right)_{j,k}^{n}$$
$$+\frac{\Delta t}{4}\left[\left(y_D-y_G\right)^2-\left(y_F-y_G\right)^2\right]\left(f_{my}\right)_{j,k}^{n}$$
$$-\frac{(\Delta t)^2}{8}\left(y_D-y_F\right)\left(f_{mt}\right)_{j,k}^{n}$$
$$+\frac{\Delta t}{2}\left(x_F-x_D\right)\left(g_m\right)_{j,k}^{n}$$
$$+\frac{\Delta t}{4}\left[\left(x_F-x_G\right)^2-\left(x_D-x_G\right)^2\right]\left(g_{mx}\right)_{j,k}^{n}$$
$$+\frac{\Delta t}{4}\left[\left(x_F-x_G\right)\left(y_F-y_G\right)-\left(x_D-x_G\right)\left(y_D-y_G\right)\right]\left(g_{my}\right)_{j,k}^{n}$$
$$-\frac{(\Delta t)^2}{8}\left(x_F-x_D\right)\left(g_{mt}\right)_{j,k}^{n}+\left(flux_m\right)_3^{n-1/2}=0\,, \tag{3.30}$$

where S_{q3} is the area of the quadrilateral $D'E'F'G'$, and $\left(x_{q3},y_{q3}\right)$ is the spatial coordinates of its centroid.

In Eq. (3.30), the fluxes leaving the three surfaces of $SE(j3,k3,n-1/2)$ is

$$
\begin{aligned}
(flux_m)_3^{n-1/2} = & \\
& -S_{q3}\left[(u_m)_{j3,k3}^{n-1/2} + (x_{q3}-x_E)(u_{mx})_{j3,k3}^{n-1/2} \right. \\
& \qquad \left. + (y_{q3}-y_E)(u_{my})_{j3,k3}^{n-1/2}\right] \\
& + \frac{\Delta t}{2}(y_F-y_D)(f_m)_{j3,k3}^{n-1/2} \\
& + \frac{\Delta t}{4}\left[(x_F-x_E)(y_F-y_E)\right. \\
& \qquad \left. -(x_D-x_E)(y_D-y_E)\right](f_{mx})_{j3,k3}^{n-1/2} \\
& + \frac{\Delta t}{4}\left[(y_F-y_E)^2-(y_D-y_E)^2\right](f_{my})_{j3,k3}^{n-1/2} \\
& + \frac{(\Delta t)^2}{8}(y_F-y_D)(f_{mt})_{j3,k3}^{n-1/2} \\
& + \frac{\Delta t}{2}(x_D-x_F)(g_m)_{j3,k3}^{n-1/2} \\
& + \frac{\Delta t}{4}\left[(x_D-x_E)^2-(x_F-x_E)^2\right](g_{mx})_{j3,k3}^{n-1/2} \\
& + \frac{\Delta t}{4}\left[(x_D-x_E)(y_D-y_E)\right. \\
& \qquad \left. -(x_F-x_E)(y_F-y_E)\right](g_{my})_{j3,k3}^{n-1/2} \\
& + \frac{(\Delta t)^2}{8}(x_D-x_F)(g_{mt})_{j3,k3}^{n-1/2}. \qquad (3.31)
\end{aligned}
$$

For each m =1, 2,…., 8, Eqs. (3.27), (3.28) and (3.30) are the three equations, which could be used to solve for the three unknowns, $(u_m)_{j,k}^n$, $(u_{mx})_{j,k}^n$ and $(u_{my})_{j,k}^n$.

The spatial coordinates of point *G*, i.e., the centroid of the hexagon *ABCDEF*, shown in Figs. 1a, can be expressed as

$$
\begin{aligned}
x_G &= \frac{S_{q1}x_{q1}+S_{q2}x_{q2}+S_{q3}x_{q3}}{S_{q1}+S_{q2}+S_{q3}} \\
y_G &= \frac{S_{q1}y_{q1}+S_{q2}y_{q2}+S_{q3}y_{q3}}{S_{q1}+S_{q2}+S_{q3}}
\end{aligned}
\qquad (3.32)
$$

Aided by Eqs. (3.32), the summation of Eqs. (3.27), (3.28) and (3.30) is

$$
\begin{aligned}
& (u_m)_{j,k}^n = \\
& -\frac{(flux_m)_1^{n-1/2}+(flux_m)_2^{n-1/2}+(flux_m)_3^{n-1/2}}{S_{q1}+S_{q2}+S_{q3}}.
\end{aligned}
\qquad (3.33)
$$

Equation (3.33) is equivalent to imposing the space-time flux conservation, i.e., Eq. (3.7) over $CE(j,k,n)$. In what follows, we deal with the calculation of the spatial derivatives of the flow variables, i.e., $(u_{mx})_{j,k}^n$ and $(u_{my})_{j,k}^n$.

To proceed, we subtract Eq. (3.27) from Eq. (3.28), and have

$$
\begin{aligned}
& \sum_{l=1}^{8}(a1_{ml})_{j,k}^n(u_{lx})_{j,k}^n + \sum_{l=1}^{8}(b1_{ml})_{j,k}^n(u_{ly})_{j,k}^n \\
& = (c1_m)_{j,k}^n, \qquad (3.34)
\end{aligned}
$$

where m,l = 1, 2, 3,…, 8. In Eq. (3.34), $(a1_{ml})_{j,k}^n$ and $(b1_{ml})_{j,k}^n$ are 8×8 matrices and $(c1_m)_{j,k}^n$ is a 8×1 column vector, and they can be expressed as

$$
\begin{aligned}
(a1_{ml})_{j,k}^n = & \\
& \left[S_{q2}(x_{q2}-x_G)-S_{q1}(x_{q1}-x_G)\right]\delta_{ml} \\
& + \frac{\Delta t}{4}(f_{m,l})_{j,k}^n\left[2(y_B-y_G)(x_B-x_G)\right. \\
& \left. -(y_D-y_G)(x_D-x_G)-(y_F-y_G)(x_F-x_G)\right] \\
& + \frac{\Delta t}{4}\left[(x_D-x_G)^2+(x_F-x_G)^2\right. \\
& \qquad \left. -2(x_B-x_G)^2\right](g_{m,l})_{j,k}^n \\
& - \frac{(\Delta t)^2}{8}(y_D+y_F-2y_B)\sum_{p=1}^{8}(f_{m,p})_{j,k}^n(f_{p,l})_{j,k}^n \\
& - \frac{(\Delta t)^2}{8}(2x_B-x_D-x_F)\sum_{p=1}^{8}(g_{m,p})_{j,k}^n(f_{p,l})_{j,k}^n
\end{aligned}
\qquad (3.35)
$$

$$
\begin{aligned}
(b1_{ml})_{j,k}^n = & \\
& \left[S_{q2}(y_{q2}-y_G)-S_{q1}(y_{q1}-y_G)\right]\delta_{ml} \\
& + \frac{\Delta t}{4}\left[2(y_B-y_G)^2-(y_D-y_G)^2\right. \\
& \qquad \left. -(y_F-y_G)^2\right](f_{m,l})_{j,k}^n \\
& + \frac{\Delta t}{4}(g_{m,l})_{j,k}^n\left[(x_D-x_G)(y_D-y_G)\right.
\end{aligned}
$$

$$+(x_F-x_G)(y_F-y_G)-2(x_B-x_G)(y_B-y_G)]$$
$$-\frac{(\Delta t)^2}{8}(y_D+y_F-2y_B)\sum_{p=1}^{8}(f_{m,p})_{j,k}^{n}(g_{p,l})_{j,k}^{n}$$
$$-\frac{(\Delta t)^2}{8}(2x_B-x_D-x_F)\sum_{p=1}^{8}(g_{m,p})_{j,k}^{n}(g_{p,l})_{j,k}^{n} \tag{3.36}$$

and

$$(c1_m)_{j,k}^{n}=(flux_m)_1^{n-1/2}-(flux_m)_2^{n-1/2}+(S_{q1}-S_{q2})(u_m)_{j,k}^{n}-\frac{\Delta t}{2}(2y_B-y_D-y_F)(f_m)_{j,k}^{n}-\frac{\Delta t}{2}(x_D+x_F-2x_B)(g_m)_{j,k}^{n} \tag{3.37}$$

Similarly, we subtract Eq. (3.27) from Eq. (3.30), and we have

$$\sum_{l=1}^{8}(a2_{ml})_{j,k}^{n}(u_{lx})_{j,k}^{n}+\sum_{l=1}^{8}(b2_{ml})_{j,k}^{n}(u_{ly})_{j,k}^{n}=(c2_m)_{j,k}^{n}, \tag{3.38}$$

where

$$(a2_{ml})_{j,k}^{n}=[S_{q3}(x_{q3}-x_G)-S_{q1}(x_{q1}-x_G)]\delta_{ml}+\frac{\Delta t}{4}(f_{m,l})_{j,k}^{n}[(y_B-y_G)(x_B-x_G)+(y_D-y_G)(x_D-x_G)-2(y_F-y_G)(x_F-x_G)]+\frac{\Delta t}{4}[2(x_F-x_G)^2-(x_B-x_G)^2-(x_D-x_G)^2](g_{m,l})_{j,k}^{n}-\frac{(\Delta t)^2}{8}(2y_F-y_B+y_D)\sum_{p=1}^{8}(f_{m,p})_{j,k}^{n}(f_{p,l})_{j,k}^{n}-\frac{(\Delta t)^2}{8}(x_B+x_D-2x_F)\sum_{p=1}^{8}(g_{m,p})_{j,k}^{n}(f_{p,l})_{j,k}^{n} \tag{3.39}$$

$$(b2_{ml})_{j,k}^{n}=[S_{q3}(y_{q3}-y_G)-S_{q1}(y_{q1}-y_G)]\delta_{ml}+\frac{\Delta t}{4}(f_{m,l})_{j,k}^{n}[(y_B-y_G)^2+(y_D-y_G)^2-2(y_F-y_G)^2]+\frac{\Delta t}{4}(g_{m,l})_{j,k}^{n}[2(x_F-x_G)(y_F-y_G)-(x_B-x_G)(y_B-y_G)-(x_D-x_G)(y_D-y_G)]-\frac{(\Delta t)^2}{8}(2y_F-y_B-y_D)\sum_{p=1}^{8}(f_{m,p})_{j,k}^{n}(g_{p,l})_{j,k}^{n}-\frac{(\Delta t)^2}{8}(x_B+x_D-2x_F)\sum_{p=1}^{8}(g_{m,p})_{j,k}^{n}(g_{p,l})_{j,k}^{n} \tag{3.40}$$

and

$$(c2_m)_{j,k}^{n}=(flux_m)_1^{n-1/2}-(flux_m)_3^{n-1/2}+(S_{q1}-S_{q3})(u_m)_{j,k}^{n}-\frac{\Delta t}{2}(y_B+y_D-2y_F)(f_m)_{j,k}^{n}-\frac{\Delta t}{2}(2x_F-x_B-x_D)(g_m)_{j,k}^{n}. \tag{3.41}$$

For each m = 1, 2,…., 8, Eqs. (3.34) and (3.38) provide two equations for two unknowns, i.e., $(u_{mx})_{j,k}^{n}$ and $(u_{my})_{j,k}^{n}$.

The combination of Eq. (3.33) for $(u_m)_{j,k}^{n}$ and Eqs. (3.34) and (3.38) for $(u_{mx})_{j,k}^{n}$ and $(u_{my})_{j,k}^{n}$ is the *a* scheme of the two-dimensional CESE method. In what follows, $(u_{mx})_{j,k}^{n}$ and $(u_{my})_{j,k}^{n}$ calculated by the *a* scheme, i.e., Eqs. (3.34) and (3.38), are referred to as $(u_{mx}^{a})_{j,k}^{n}$ and $(u_{my}^{a})_{j,k}^{n}$. For solutions with discontinuities, further modification for the calculation of $(u_{mx})_{j,k}^{n}$ and $(u_{my})_{j,k}^{n}$ is needed, while the calculation of $(u_m)_{j,k}^{n}$ does not change in this extension. The present two-dimensional *a* scheme will be extended to the *a*-ε and the *a*-ε-α-β schemes.

To proceed, for *m = 1, 2,…., 8,* flow variables at G', $(u_m)_{j,k}^{n}$, is obtained from Eq. (3.33). Flow variables $(u_m')_{j1,k1}^{n}$, $(u_m')_{j2,k2}^{n}$ and $(u_m')_{j3,k3}^{n}$ at points A', C' and E', respectively, are calculated by a first-order Taylor series expansion

$$\left(u_m^{'}\right)_{jr,kr}^{n} = \left(u_m\right)_{jr,kr}^{n-1/2} + \frac{\Delta t}{2}\left(u_{mt}\right)_{jr,kr}^{n-1/2}, \qquad (3.42)$$

for r = 1, 2, 3. Refer to Fig 1e. Based on $\left(u_m^{'}\right)_{j1,k1}^{n}$, $\left(u_m^{'}\right)_{j2,k2}^{n}$ and $\left(u_m^{'}\right)_{j3,k3}^{n}$ on points $A^{'}$, $C^{'}$ and $E^{'}$, we apply central differencing to calculate $\left(u_{mx}\right)_{j,k}^{n}$ and $\left(u_{my}\right)_{j,k}^{n}$ as

$$\left(u_{mx}^{c}\right)_{j,k}^{n} = \frac{1}{2S_{ACE}}\left[\left(y_C - y_E\right)\left(u_m^{'}\right)_{j1,k1}^{n} + \left(y_E - y_A\right)\left(u_m^{'}\right)_{j2,k2}^{n} + \left(y_A - y_C\right)\left(u_m^{'}\right)_{j3,k3}^{n}\right], \qquad (3.43)$$

and

$$\left(u_{my}^{c}\right)_{j,k}^{n} = \frac{1}{2S_{ACE}}\left[\left(x_E - x_C\right)\left(u_m^{'}\right)_{j1,k1}^{n} + \left(x_A - x_E\right)\left(u_m^{'}\right)_{j2,k2}^{n} + \left(x_C - x_A\right)\left(u_m^{'}\right)_{j3,k3}^{n}\right]. \qquad (3.44)$$

Similar central differencing can be applied to calculate $\left(u_{mx}^{(1)}\right)_{j,k}^{n}$ and $\left(u_{my}^{(1)}\right)_{j,k}^{n}$ for $\Delta C^{'}E^{'}G^{'}$, $\left(u_{mx}^{(2)}\right)_{j,k}^{n}$ and $\left(u_{my}^{(2)}\right)_{j,k}^{n}$ for $\Delta A^{'}G^{'}E^{'}$, and $\left(u_{mx}^{(3)}\right)_{j,k}^{n}$ and $\left(u_{my}^{(3)}\right)_{j,k}^{n}$ for $\Delta A^{'}C^{'}G^{'}$. Moreover, because point $G^{'}$ is the centroid of $\Delta A^{'}C^{'}E^{'}$, one could easily show that

$$\left(u_{mx}^{c}\right)_{j,k}^{n} = \frac{1}{3}\sum_{r=1}^{3}\left(u_{mx}^{(r)}\right)_{j,k}^{n}, \quad \left(u_{my}^{c}\right)_{j,k}^{n} = \frac{1}{3}\sum_{r=1}^{3}\left(u_{my}^{(r)}\right)_{j,k}^{n}. \qquad (3.45)$$

Aided by Eqs. (3.43-44), $\left(u_{mx}\right)_{j,k}^{n}$ and $\left(u_{my}\right)_{j,k}^{n}$ for the a-ε scheme are

$$\left(u_{mx}\right)_{j,k}^{n} = \left(u_{mx}^{a}\right)_{j,k}^{n} + 2\varepsilon\left[\left(u_{mx}^{c}\right)_{j,k}^{n} - \left(u_{mx}^{a}\right)_{j,k}^{n}\right], \qquad (3.46)$$

$$\left(u_{my}\right)_{j,k}^{n} = \left(u_{my}^{a}\right)_{j,k}^{n} + 2\varepsilon\left[\left(u_{my}^{c}\right)_{j,k}^{n} - \left(u_{my}^{a}\right)_{j,k}^{n}\right], \qquad (3.47)$$

for m = 1, 2,…., 8. For numerical stability we must have $0 \le \varepsilon \le 1$.

For the a-ε-α-β scheme, $\left(u_{mx}\right)_{j,k}^{n}$ and $\left(u_{my}\right)_{j,k}^{n}$ are

$$\left(u_{mx}\right)_{j,k}^{n} = \left(u_{mx}^{a}\right)_{j,k}^{n} + 2\varepsilon\left[\left(u_{mx}^{c}\right)_{j,k}^{n} - \left(u_{mx}^{a}\right)_{j,k}^{n}\right] + \beta\left[\left(u_{mx}^{w}\right)_{j,k}^{n} - \left(u_{mx}^{c}\right)_{j,k}^{n}\right], \qquad (3.48)$$

$$\left(u_{my}\right)_{j,k}^{n} = \left(u_{my}^{a}\right)_{j,k}^{n} + 2\varepsilon\left[\left(u_{my}^{c}\right)_{j,k}^{n} - \left(u_{my}^{a}\right)_{j,k}^{n}\right] + \beta\left[\left(u_{my}^{w}\right)_{j,k}^{n} - \left(u_{my}^{c}\right)_{j,k}^{n}\right], \qquad (3.49)$$

for m = 1, 2,…., 8. For numerical stability, we have $\beta \ge 0$. In Eqs. (3.48-49), $\left(u_{mx}^{w}\right)_{j,k}^{n}$ and $\left(u_{my}^{w}\right)_{j,k}^{n}$ are defined as,

$$\left(u_{mx}^{w}\right)_{j,k}^{n} = \frac{1}{\omega}\left[\left(\theta_{m2}\theta_{m3}\right)^{\alpha}\left(u_{mx}^{(1)}\right)_{j,k}^{n} + \left(\theta_{m1}\theta_{m3}\right)^{\alpha}\left(u_{mx}^{(2)}\right)_{j,k}^{n} + \left(\theta_{m1}\theta_{m2}\right)^{\alpha}\left(u_{mx}^{(3)}\right)_{j,k}^{n}\right] \qquad (3.50)$$

$$\left(u_{my}^{w}\right)_{j,k}^{n} = \frac{1}{\omega}\left[\left(\theta_{m2}\theta_{m3}\right)^{\alpha}\left(u_{my}^{(1)}\right)_{j,k}^{n} + \left(\theta_{m1}\theta_{m3}\right)^{\alpha}\left(u_{my}^{(2)}\right)_{j,k}^{n} + \left(\theta_{m1}\theta_{m2}\right)^{\alpha}\left(u_{my}^{(3)}\right)_{j,k}^{n}\right] \qquad (3.51)$$

for m = 1, 2,…., 8, where

$$\theta_{mr} = \left[\sqrt{\left(u_{mx}^{(r)}\right)^2 + \left(u_{my}^{(r)}\right)^2}\right]_{j,k}^{n}, \qquad (3.52)$$

for r = 1, 2, 3. And

$$\omega = \left(\theta_{m1}\theta_{m2}\right)^{\alpha} + \left(\theta_{m2}\theta_{m3}\right)^{\alpha} + \left(\theta_{m1}\theta_{m3}\right)^{\alpha}. \qquad (3.53)$$

This concludes the discussion of the two-dimensional $a-\varepsilon-\alpha-\beta$ scheme, used for numerical analysis of the benchmark MHD flows in the present paper. Because the spatial derivatives of flow variables are unknowns, we need to specify their initial values and boundary values. In all calculated flows presented in the present paper, the parameters ε, α and β are set to half, unity and unity, respectively.

4. Results and Discussions

In this section, we shall do two-dimensional calculations based on rotated one-dimensional problems. In a one-dimensional problem, $\nabla \cdot \mathbf{B} = 0$ is automatically satisfied by setting B_x to be a constant. By rotating the coordinates with a non-zero angle, the one-dimensional problem becomes two-dimensional. As such, the constraint $\nabla \cdot \mathbf{B} = 0$ may not be easily maintained numerically. The effect of violating $\nabla \cdot \mathbf{B} = 0$ in numerical results can be judged by the comparison between the two-dimensional results with the corresponding one-dimensional results. Previously, this approach has been adopted by [2, 4, 6,7, 9].

Moreover, we define the following error measurement to assess the divergence free constraint for the magnetic field,

$$Error = \frac{\sum_{j=1}^{N}\sum_{k=1}^{M}\left|\left(\nabla \cdot \mathbf{B}\right)_{j,k}\right|}{N \times M}, \tag{4.1}$$

Note that the spatial domain is descritized by a $N \times M$ mesh, and $\left(\nabla \cdot \mathbf{B}\right)_{j,k}$ in Eq. (4.1) is defined by using Gauss' divergence theorem. For example,

$$\left(\nabla \cdot \mathbf{B}\right)_{j,k} = \frac{\int_{ABCDEF} \nabla \cdot \mathbf{B} d\sigma}{\int_{ABCDEF} d\sigma} = \frac{\oint_{ABCDEF} \mathbf{B} d\mathbf{s}}{\int_{ABCDEF} d\sigma}, \tag{4.2}$$

As presented in Fig. 1, Points *A, B, C, D, E* and *F* form a hexagon in the spatial plane. Equation (4.2) is an area average of $\nabla \cdot \mathbf{B}$ over a spatial cell, i.e., hexagon *ABCDEF*.

4.1 A Smooth Alfven Wave

The smooth Alfven wave problem was proposed in [9]. We adopt this flow to test the capabilities of the CESE method in keeping the constraint $\nabla \cdot \mathbf{B} = 0$ for flows of smooth solutions. To proceed, we let ξ be the coordinate of the original one-dimensional problem and η as the coordinate perpendicular to ξ. The Alfven wave propagates in the ξ direction at the speed of $v_a = B_\xi \big/ \sqrt{\rho} = -1$. Let $v_a + u_\xi = 0$, and the wave becomes a standing wave and the solution is

$$\begin{aligned}
&\rho = 1, \\
&p = 0.1, \\
&u_\xi = 1, \\
&u_\eta = 0.1\sin(2\pi\xi), \\
&w = 0.1\cos(2\pi\xi), \\
&B_\xi = 1, \\
&B_\eta = 0.1\sin(2\pi\xi), \\
&B_z = 0.1\cos(2\pi\xi),
\end{aligned} \tag{4.3}$$

with $\gamma = 5/3$. We rotate the coordinates with the angle ϕ and let the new coordinates be (*x, y*). Refer to Fig. 2. The relation between the two sets of the coordinates is

$$\begin{pmatrix} \xi \\ \eta \end{pmatrix} = \mathbf{T}\begin{pmatrix} x \\ y \end{pmatrix}, \tag{4.4}$$

where

$$\mathbf{T} = \begin{pmatrix} \cos\phi & \sin\phi \\ -\sin\phi & \cos\phi \end{pmatrix} \quad \text{and} \quad \mathbf{T}^{-1} = \begin{pmatrix} \cos\phi & -\sin\phi \\ \sin\phi & \cos\phi \end{pmatrix}. \tag{4.5}$$

The numerical calculation is performed in the *x*-*y* coordinates and the computational domain is rectangular. Refer to OABC in Fig. 2. The size of domain is $x \in [0, 1/\cos\phi]$ and $y \in [0, 1/\sin\phi]$. In the present paper, ϕ is set at 60^o and three meshes are used: 33×65, 17×33 and 9×17. The corresponding time steps are set to 0.01, 0.02 and 0.05. Periodic boundary condition is imposed in both *x*- and *y*-directions. Because there is no shock, α in the CESE method is set to be null.

The initial conditions of vector variables in *x*-*y* coordinate are obtained by coordinate transformation as,

$$\begin{pmatrix} B_x \\ B_y \end{pmatrix} = \mathbf{T}^{-1}\begin{pmatrix} B_\varsigma \\ B_\eta \end{pmatrix} \text{ and } \begin{pmatrix} u \\ v \end{pmatrix} = \mathbf{T}^{-1}\begin{pmatrix} u_\varsigma \\ u_\eta \end{pmatrix}. \tag{4.6}$$

Aided by Eqs. (4.3-6), the initial flow conditions in *x*-*y* coordinate can be expressed as functions of spatial variables *x* and *y*. Moreover, the spatial derivatives of the flow variables can also be obtained. After the calculation, i.e., *t = 5,* flow variables are converted to be in the ξ-η coordinate through the simple coordinate transformation, Eq. (4.6).

Figure 3a shows the profile of B_η along the line of y = 0 with different mesh resolution. The errors in the wave amplitude are quickly reduced with the use of a refined mesh. The solution obtained by the mesh of 33×65 is nearly identical to the analytical solution. We remark that there is no phase error in the result because the solution is a standing wave. Figure 3b shows the *Error* with respect to different mesh resolution for assessing the divergence free constraint for the magnetic field. The *Error*, defined in Eq. (4.1), is confined to at a very small magnitude and remains at the same level for the whole computational time.

To investigate the numerical solution of a traveling wave, we let $u_\xi = 0$. Refer to Eq. (4.3). The Alfven wave moves to towards the origin, i.e., (x, y) = (0, 0), along the ξ direction. Due to the periodic condition, the wave returns to its initial position by t = 1. Figure 4a shows the profile of B_η along the line of y = 0 with different mesh resolution. The errors in phase and amplitude is reduced with higher mesh resolution. Figures 4b shows the *Error*, Eq. (4.1), for assessing the divergence free condition of the magnetic field with different mesh resolution. No accumulation of *Error* can be observed during the evolution of the flow solution.

The above results show that for the smooth solutions the CESE method without using any additional numerical treatment can automatically keeps the constraint of $\nabla \cdot \mathbf{B} = 0$ in a satisfactory fashion.

4.2 Rotated Brio and Wu's One-Dimensional Test

Brio and Wu's one-dimensional benchmark test [1] is solved in a two-dimensional domain through the use of coordinate rotation as illustrated in Section 4.1. Three meshes are used: 99×199, 199×399 and 399×799. The rotation angle is set to 45°. The computational domain is, $x \in [0, \sqrt{2}/2]$ and $y \in [0, \sqrt{2}/2]$. The initial condition along the ξ-direction is

$$\left(\rho, u, v, w, p, B_\eta, B_z\right) = \begin{cases} (\,1.000,\ 0,\ 0,\ 0,\ 1.0,\ +1,\ 0\,) & \text{for } \xi < 0.5 \\ (\,0.125,\ 0,\ 0,\ 0,\ 0.1,\ -1,\ 0\,) & \text{for } \xi > 0.5 \end{cases} \quad (4.7)$$

with $B_\xi = 0.75$ and $\gamma = 2$. Through a simple coordinate transformation, Eq. (4.6), the initial profiles of velocity and magnetic fields in the x-y coordinates are obtained. Non-reflect boundary condition along η-direction (y = -x) is applied to the computational boundary. Δt and α are set to 0.0001 and 1, respectively.

For comparison with the one-dimensional results in [17], the two-dimensional results in x-y coordinates at t = 0.1 are transformed to ξ-η coordinates. Figures 5a-e show the comparison between one-dimensional results and two-dimensional results, using a 399×799 mesh. In Figs. 5a-e, one-dimensional results in [17] are plotted by lines and two-dimensional results are plotted by dots. By using the CESE method, the two-dimensional results are in favorable agreement with the one-dimensional ones and no special treatment has been used to enforce the divergence-free constraint for the magnetic field.

Analytically, the component B_ξ should be a constant along ξ direction during evolution of waves. Figures 6a-h show its numerical solution with a mesh of 399×799 grid points at *t= 0.001, 0.004, 0.007, 0.01, 0.02, 0.04, 0.06* and *0.10,* respectively. Some oscillations are observed in the profile of B_ξ , but the effect on results is small as shown in Fig. 5. Figure 7 shows the evolution of *Error* in Eq. (4.1) with different mesh resolution. Starting from very small value, the error increased to about 10^{-1} due to the solution discontinuities and remained nearly at the same level during the solution evolution. Figures 8 show the distribution of B_ξ at t = 0.1 with different mesh resolution. Figures 9 show the distribution of density at t = 0.1 with different mesh resolution. For this flow with solution discontinuities, we demonstrated that the results by the two-dimensional CESE method are in good agreement with the one-dimensional solutions without using any special treatment to numerically satisfy the constraint $\nabla \cdot \mathbf{B} = 0$. The $\nabla \cdot \mathbf{B} = 0$ is violated mainly in the regions near shocks and the values of $|\nabla \cdot \mathbf{B}|$ is bounded as shown in Fig. 7.

5. Concluding Remarks

In this paper, we reported the extension of the CESE method to calculate the ideal MHD equations in two spatial dimensions. Contrast to the modern upwind schemes, the present approach has much simpler logics and operational counts because no reconstruction procedure or Riemann solver is needed. We also use the CESE method to solve multi-dimensional MHD equations without special treatment for remaining the constraint of $\nabla \cdot \mathbf{B} = 0$. With the CESE method, the $\nabla \cdot \mathbf{B} = 0$ constraint has been faithfully maintained in smooth region. For region with shocks, the orders

$|\nabla \cdot \mathbf{B}|$ of are bounded. No stability problem is encountered in present computation. Two standard MHD problems have been solved. In all cases, numerical results by the CESE method compared favorably with that obtained by using the higher order modern upwind schemes. Present research has paved the way to solve more complex non-ideal MHD equations.

References

1. M. Brio and C. C. Wu, "An upwind difference scheme for the equations of ideal magnetohydrodynamics", *Journal of Computational Physics.* Vol. 75, 1988, pp. 400-422.
2. G. -S. Jiang and C. C. Wu, "A high-order WENO finite difference scheme for the equations of ideal magnetohydrodynamics", *Journal of Computational Physics.* Vol. 150, 1999, pp. 561-594.
3. J .P. Brackbill and D.C. Barnes, "The effect of nonzero $\nabla \cdot \mathbf{B}$ on the numerical solution of the magnetohydrodynamic equations", *Journal of Computational Physics,* vol. 35, 1980, pp. 426-432.
4. K. G. Powell, "An approximate Riemann solver for magneto-hydro-dynamics", ICASE Report 94-24, 1994.
5. C .R. Evans and J. F. Hawley, "Simulation of magnetohydrodynamic flows: a constrained transport method", *Astrophysical Journal*, vol. 332, 1988, pp.659-677.
6. W. Dai and P. R. Woodward, "A simple finite difference scheme for multidimensional magnetohydrodanamical equations", *Journal of Computational Physics,* vol. 141, 1998, pp. 331-369.
7. D. Ryu, F. Miniati, T. W. Jones and A. Frank, "A divergence-free upwind code for multidimensional magnetohydrodynamic flows", *Astrophysical Journal*, vol. 509, 1998, 244-255.
8. D. S. Balsara and D. S. Spice, "A staggered mesh algorithm using high order Godunov fluxs to ensure solenoidal magnetic fields in magnetohydrodynamic simulations", *Journal of Computational Physics,* vol. 149, 1999, pp. 270-292.
9. G. Tóth, "The Constraint $\nabla \cdot \mathbf{B} = 0$ in shock capturing magnetohydrodynamics codes", *Journal of Computational Physics,* vol. 161, 2000, pp. 605-652.
10. H. -Z. Tang and K. Xu, "A high-order Gas-Kinetic Method for multidimensional ideal magnetohydrodynamics", *Journal of Computational Physics,* vol. 165, 2000, pp. 69-88.
11. S.C. Chang and W. M. To, "A New Numerical Framework for Solving Conservation Laws – The Method of Space-Time Conservation Element and Solution Element", NASA TM 104498, 1991.
12. S. C. Chang, "The Method of Space-time Conservation Element and Solution Element–A New Approach for Solving the Navier-Stokes and the Euler Equations", *Journal of Computational Physics,* vol. 119, 1995, pp 295-324.
13. S. C. Chang X.Y. Wang and C.Y. Chow, "The Space-Time Conservation Element and Solution Element Method: A New High-Resolution and Genuinely Multidimensional Paradigm for Solving Conservation Laws", *Journal of Computational Physics,* 156, 1999, pp. 89-136.
14. X. Y. Wang and S. C. Chang, "A 2D Non-splitting Unstructured Triangular Mesh Euler Solver Based on the Space-time Conservation Element and Solution Element Method", *Computational Fluid Dynamics Journal,* vol. 8, No. 2, 1999, pp.309-325.
15. S. C. Chang, X.Y. Wang and W.M. To, "Application of the Space-time Conservation Element and Solution Element Method to One-Dimensional Convection-Diffusion Problems", *Journal of Computational Physics,* vol. 165, 2000, pp. 189-215.
16. Z.C. Zhang, S. T. Yu and S. C. Chang, "A Space-Time Conservation Element and Solution Element Method for Solving the Two- and Three-Dimensional Unsteady Euler Equations Using Quadrilateral and Hexahedral Meshes", *Journal of Computational Physics.* Vol. 175, 2002, pp.168-199.
17. M.J. Zhang, S. C. Lin, S. T. Yu, S. C. Chang and I. Blankson, "Application of the Space-Time Conservation Element and Solution Element Method to the Ideal Magnetohydrodynamics Equations", AIAA-2002-3888, 38th AIAA/ASME/SAE/ASEE Joint Propulsion Conference & Exhibit, Indianpolis, IN, July 7-9, 2002

Appendix: The Jacobian Matrix of Two-dimensional MHD Equations

$$\mathbf{F}=\frac{\partial \mathbf{f}}{\partial \mathbf{u}}=\begin{bmatrix} 0 & 1 & 0 & 0 & 0 & 0 & 0 & 0 \\ \frac{\gamma-3}{2}u^2+\frac{\gamma-1}{2}\left(v^2+w^2\right) & (3-\gamma)u & (1-\gamma)v & (1-\gamma)w & \gamma-1 & -\gamma B_x & (2-\gamma)B_y & (2-\gamma)B_z \\ -uv & v & u & 0 & 0 & -B_y & -B_x & 0 \\ -uw & w & 0 & u & 0 & -B_z & 0 & -B_x \\ A_1 & A_2 & A_3 & A_4 & A_5 & A_6 & A_7 & A_8 \\ 0 & 0 & 0 & 0 & 0 & 0 & 0 & 0 \\ -\frac{uB_y-vB_x}{\rho} & \frac{B_y}{\rho} & -\frac{B_x}{\rho} & 0 & 0 & -v & u & 0 \\ -\frac{uB_z-wB_x}{\rho} & \frac{B_z}{\rho} & 0 & -\frac{B_x}{\rho} & 0 & -w & 0 & u \end{bmatrix}, \tag{A.1}$$

Where

$$A_1=-\gamma\frac{ue}{\rho}+(\gamma-1)u(u^2+v^2+w^2)+\frac{\gamma-2}{2}u\frac{B_y^2+B_z^2}{\rho}+\frac{\gamma}{2}u\frac{B_x^2}{\rho}+B_x\frac{vB_y+wB_z}{\rho}, \tag{A.2a}$$

$$A_2=\gamma\frac{e}{\rho}+\frac{3}{2}(1-\gamma)u^2+\frac{1-\gamma}{2}(v^2+w^2)-\frac{\gamma-2}{2}\frac{B_y^2+B_z^2}{\rho}-\frac{\gamma}{2}\frac{B_x^2}{\rho}, \tag{A.2b}$$

$$A_3=(1-\gamma)uv-\frac{B_xB_y}{\rho}, \tag{A.2c}$$

$$A_4=(1-\gamma)uw-\frac{B_xB_z}{\rho}, \tag{A.2d}$$

$$A_5=\gamma u, \tag{A.2e}$$

$$A_6=-\gamma uB_x-\left(vB_y+wB_z\right), \tag{A.2f}$$

$$A_7=-vB_x+(2-\gamma)uB_y, \tag{A.2g}$$

and

$$A_8=-wB_x+(2-\gamma)uB_z. \tag{A.2h}$$

$$\mathbf{G}=\frac{\partial \mathbf{g}}{\partial \mathbf{u}}=\begin{bmatrix} 0 & 0 & 1 & 0 & 0 & 0 & 0 & 0 \\ uv & v & u & 0 & 0 & -\gamma B_y & -\gamma B_x & 0 \\ \frac{\gamma-3}{2}v^2+\frac{\gamma-1}{2}\left(u^2+w^2\right) & (1-\gamma)u & (3-\gamma)v & (1-\gamma)w & \gamma-1 & (2-\gamma)B_x & \gamma B_y & \gamma B_z \\ -vw & 0 & w & v & 0 & 0 & -B_z & -B_y \\ B_1 & B_2 & B_3 & B_4 & B_5 & B_6 & B_7 & B_8 \\ \frac{uB_y-vB_x}{\rho} & -\frac{B_y}{\rho} & \frac{B_x}{\rho} & 0 & 0 & v & u & 0 \\ 0 & 0 & 0 & 0 & 0 & 0 & 0 & 0 \\ -\frac{vB_z-wB_y}{\rho} & 0 & \frac{B_z}{\rho} & -\frac{B_y}{\rho} & 0 & 0 & -w & v \end{bmatrix}, \tag{A.3}$$

Where

$$B_1 = -\gamma \frac{ve}{\rho} + (\gamma - 1)v(u^2 + v^2 + w^2) + \frac{\gamma - 2}{2} v \frac{B_x^2 + B_z^2}{\rho} + \frac{\gamma}{2} u \frac{B_y^2}{\rho} + B_y \frac{uB_x + wB_z}{\rho}, \tag{A.4a}$$

$$B_2 = (1 - \gamma)uv - \frac{B_x B_y}{\rho}, \tag{A.4c}$$

$$B_3 = \gamma \frac{e}{\rho} + \frac{3}{2}(1 - \gamma)v^2 + \frac{1 - \gamma}{2}(u^2 + w^2) - \frac{\gamma - 2}{2} \frac{B_x^2 + B_z^2}{\rho} - \frac{\gamma}{2} \frac{B_y^2}{\rho}, \tag{A.4b}$$

$$B_4 = (1 - \gamma)vw - \frac{B_y B_z}{\rho}, \tag{A.4d}$$

$$B_5 = \gamma v, \tag{A.4e}$$

$$B_6 = (2 - \gamma)vB_x - uB_y, \tag{A.4f}$$

$$B_7 = -\gamma v B_y - (uB_x + wB_z), \tag{A.4g}$$

and

$$B_8 = -wB_y + (2 - \gamma)vB_z. \tag{A.4h}$$

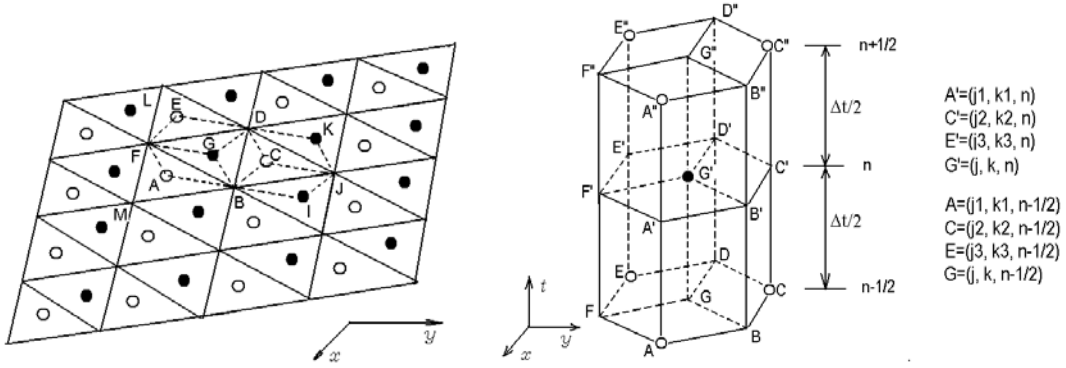

1a 1b

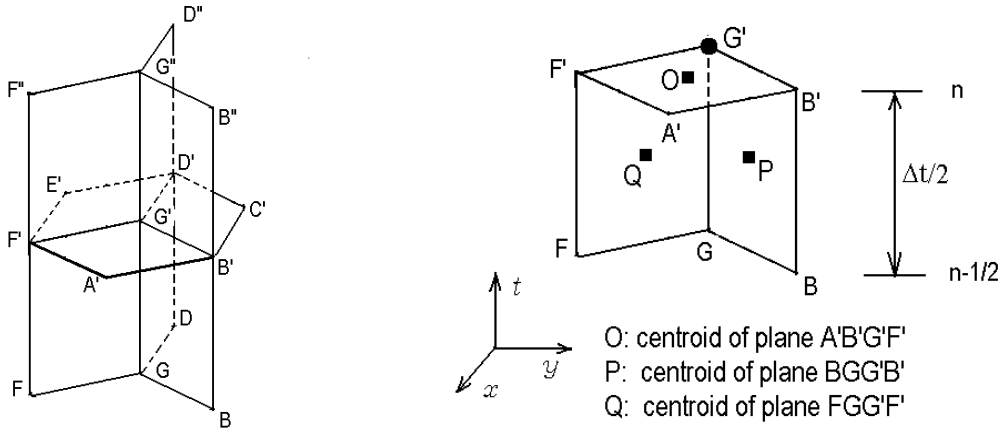

1c 1d

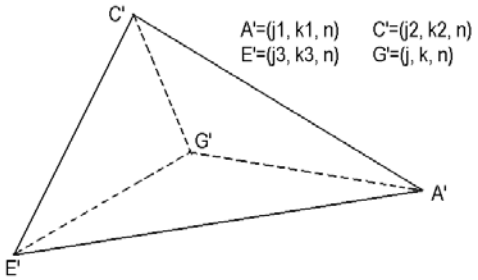

1e

Fig. 1: Definition of space-time mesh for a two-dimensional problem, Solution Elemenet (SE) and Conservation Element (CE). (a). Spatial meshes, (b) The space-time grid points arrangement. (c). $SE(j,k,n)$. (d) Three planes belonging to $SE(j,k,n)$ in $CE_1(j,k,n)$ (e) $\Delta A'C'E'$ and its centroid G'.

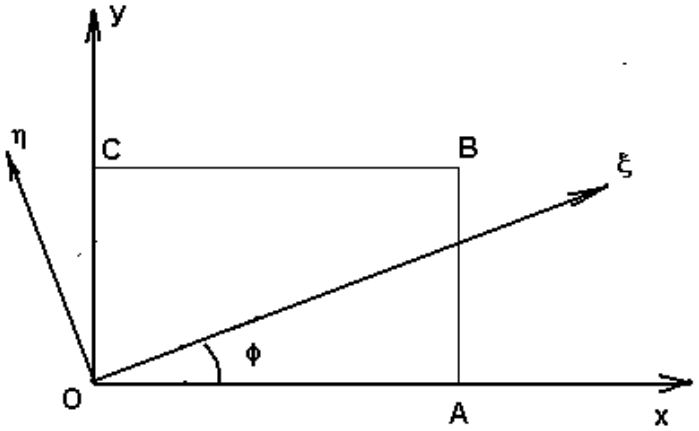

Fig. 2: Relation between x-y coordinates and ξ-η coordinates. Rectangle OABC is the computational domain.

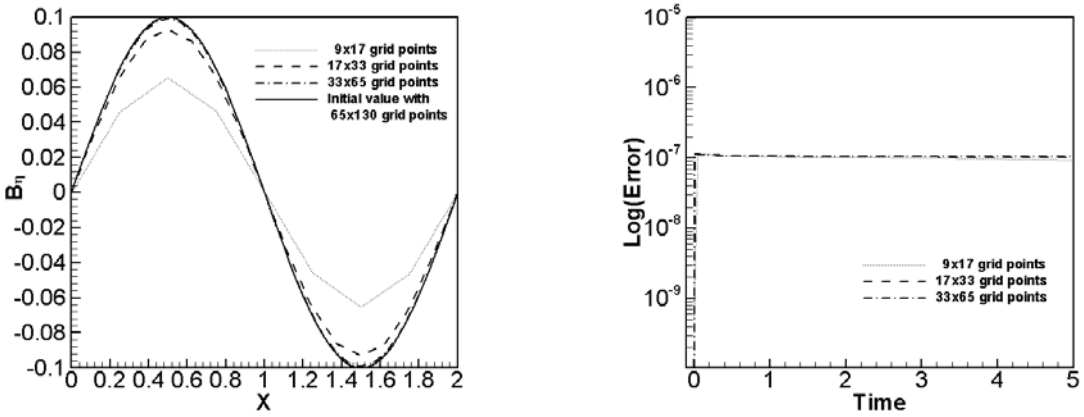

3a. 3b.

Fig. 3: A standing smooth Alfven wave proposed by Toth [9]. (a) Distribution of B_η with different mesh resolution at $t = 5$. (b) Evolution of $\nabla \cdot \mathbf{B}$ defined in Eq. (4.3) with different mesh resolution.

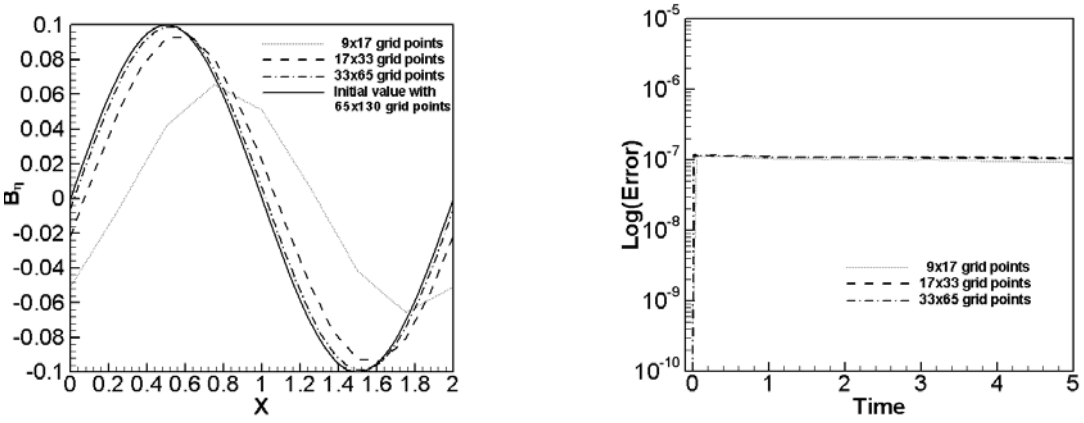

4a. 4b

Fig. 4: A traveling smooth Alfven wave proposed by Toth [9]. (a) Distribution of B_η with different mesh resolution at $t = 5$. (b) Evolution of $\nabla \cdot \mathbf{B}$ defined in Eq. (4.3) with different mesh resolution.

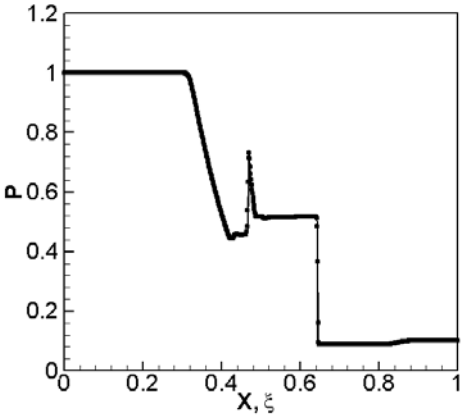

5a

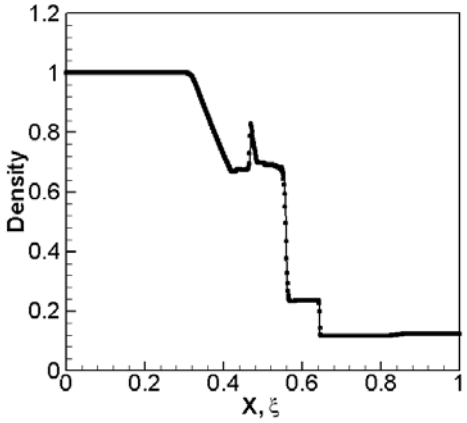

5b

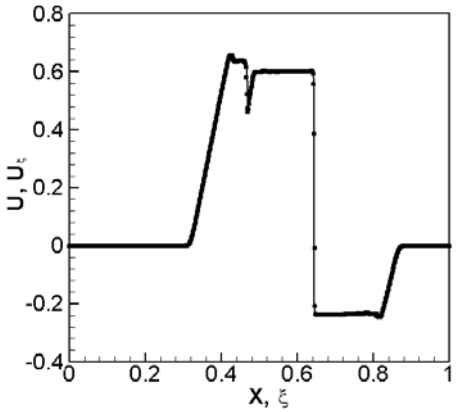

5c

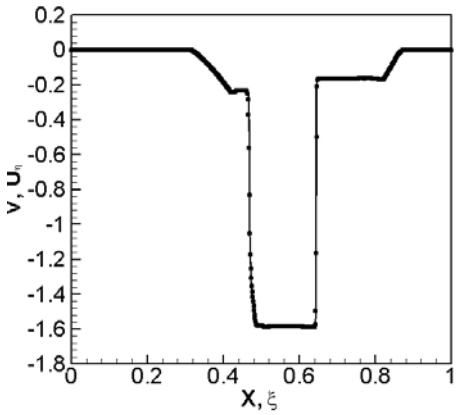

5d

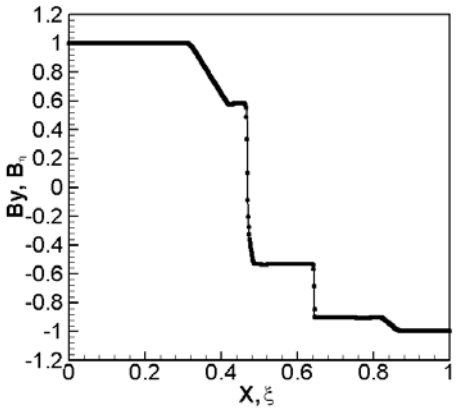

5e

Fig. 5: A Rotated one-dimensional MHD problem proposed by Brio and Wu [1] with 399x799 grid points. Comparison is between one-dimensional solution and two-dimensional solution. The one-dimensional solution in [17] is plotted by line. The two-dimensional solution is plotted by dots. (a) Pressure. (b) Density (c) Velocity *u. (*d) Velocity *v*. (e) Magnetic field B_y.

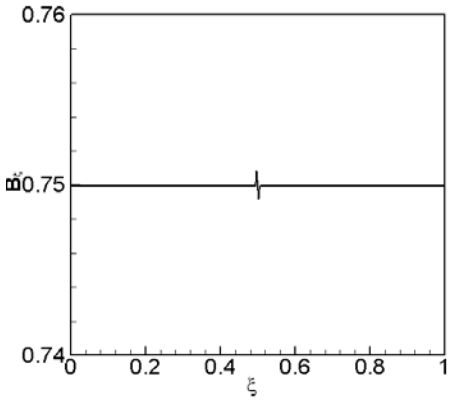

6a

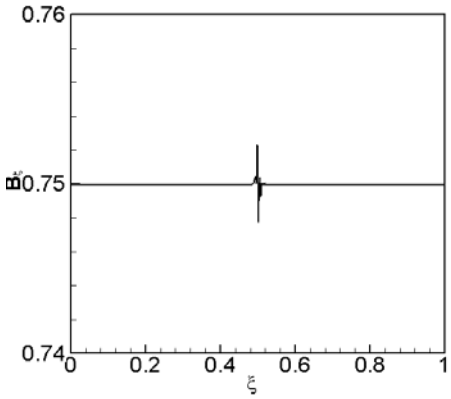

6b

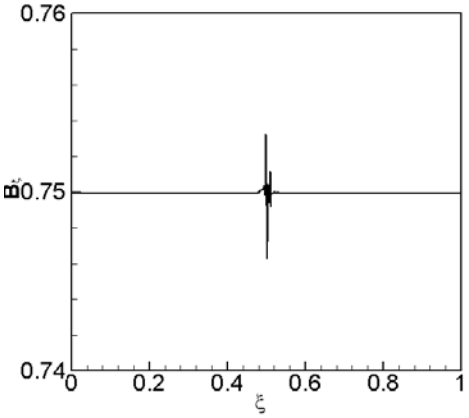

6c

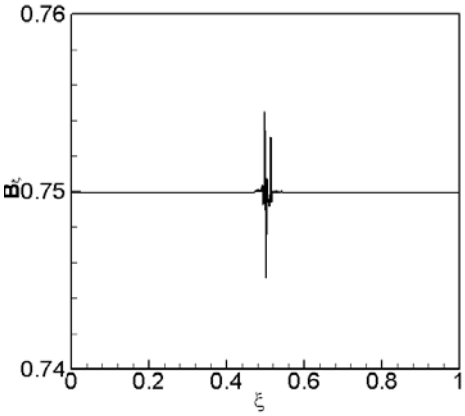

6d

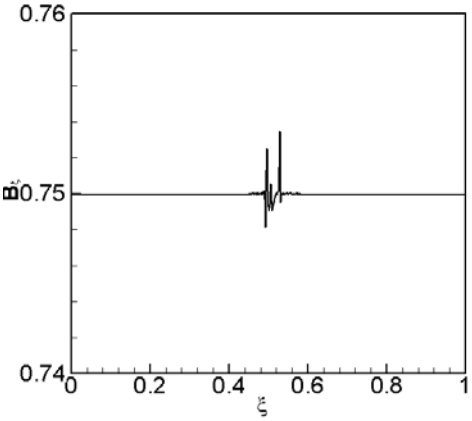

6e

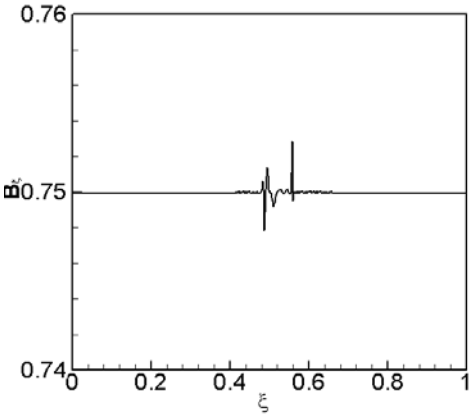

6f

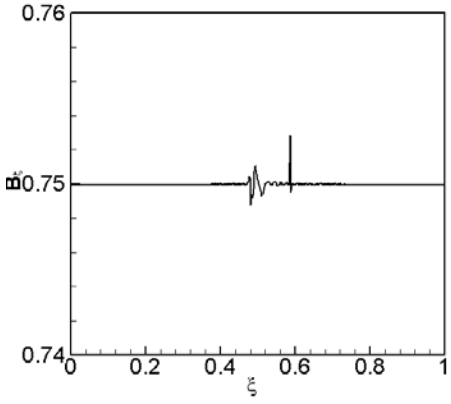

6g

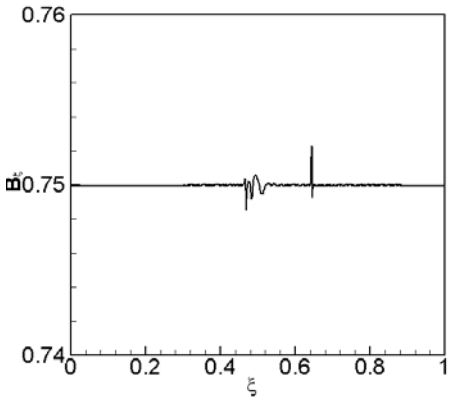

6h

Fig. 6: A rotated one-dimensional MHD problem proposed by Brio and Wu [1]. Snapshot of magnetic field B_ξ at different time with 399x799 grid points: (a) $t = 0.001$. (b) $t = 0.004$. (c) $t = 0.007$. (d) $t = 0.01$. (e) $t = 0.02$. (f) $t = 0.04$. (g) $t = 0.06$. (h) $t = 0.1$.

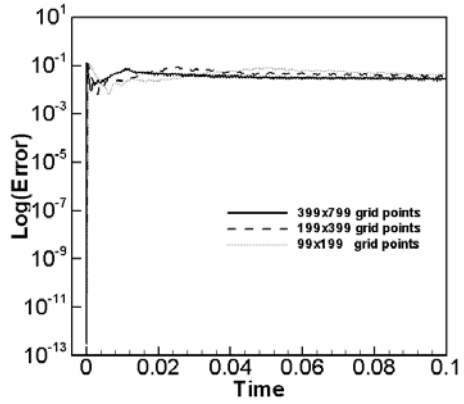

Fig. 7: A rotated one-dimensional MHD problem proposed by Brio and Wu [1]. Evolution of $\nabla \cdot \mathbf{B}$ defined in Eq. (4.3) with different mesh resolution.

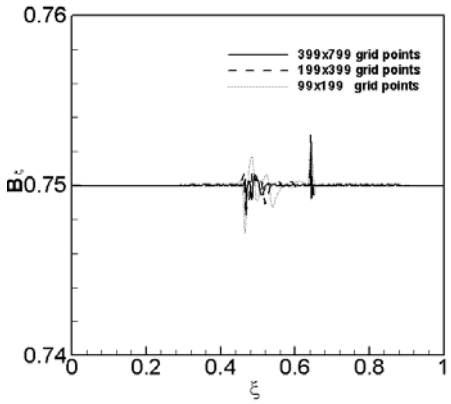

Fig. 8: A rotated one-dimensional MHD problem proposed by Brio and Wu [1]. Distribution of B_ξ at $t = 0.1$ with different mesh resolution.

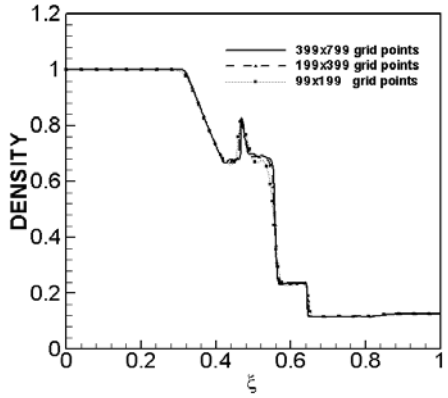

Fig. 9: A rotated one-dimensional MHD problem proposed by Brio and Wu [1]. Distribution of density at $t = 0.1$ with different mesh resolution.